Park, J., Ehrlich, R., Lühr, H., Ritter, P. (2012): Plasma irregularities in the high-latitude ionospheric F-region and their diamagnetic signatures as observed by CHAMP. - Journal of Geophysical Research, 117, A10

DOI: 10.1029/2012JA018166

Plasma irregularities in the high-latitude ionospheric F-region and their diamagnetic signatures as observed by CHAMP

Jaeheung Park,[1] Robert Ehrlich,[2] Hermann Lühr,[1] and Patricia Ritter[1]

Received 27 July 2012; revised 5 September 2012; accepted 13 September 2012; published 20 October 2012.

[1] Diamagnetic effects of ionospheric irregularities have been investigated at low-latitudes before, but no corresponding effort has been made at high latitudes. In this study we demonstrate clear diamagnetic signatures of high-latitude ionospheric irregularities as observed by the CHAMP satellite. We also present the climatology of these diamagnetic signatures for the years 2001–2010 and compare it with a previous study based on Global Positioning System (GPS) scintillation measurements. The climatology of the diamagnetic signatures is in reasonable agreement with that of the scintillations. The occurrence rate of the ionospheric irregularities generally peaks along the auroral latitudes around the pole, but it is not uniform zonally. The occurrence rate exhibits a maximum at the dayside cusp and in the pre-midnight ionosphere. The occurrence rate increases with solar and/or auroral activity. The region of high occurrence rate expands equatorward with increasing auroral activity. Occurrence probabilities are higher in local winter than in local summer. The overall occurrence rate is smallest around June solstice and largest around December solstice. The ionospheric irregularities are generally accompanied by bursts of small-scale field-aligned currents (FACs), and they are related to Region 1 FACs.

Citation: Park, J., R. Ehrlich, H. Lühr, and P. Ritter (2012), Plasma irregularities in the high-latitude ionospheric F-region and their diamagnetic signatures as observed by CHAMP, *J. Geophys. Res.*, *117*, A10322, doi:10.1029/2012JA018166.

1. Introduction

[2] Ionospheric irregularities are common phenomena of the low-latitude ionosphere during post-sunset hours [e.g., *Kil and Heelis*, 1998; *Su et al.*, 2006; *Stolle et al.*, 2006; *Xiong et al.*, 2012]. In most cases we find local plasma depletions termed equatorial plasma bubbles (EPBs). In recent years EPBs have attained a lot of attention because they can disturb radio transmission links [e.g., *Aarons et al.*, 1981; *Bhattacharyya et al.*, 2000; *Nishioka et al.*, 2011; *Seo et al.*, 2011] such as Global Positioning System (GPS) navigation signals. Also in the high-latitude ionosphere various physical processes can generate plasma density irregularities.

[3] The Tongue of Ionization (TOI) is a high-density plasma region elongated from the dayside cusp into the polar cap. The main source of TOI is sunlit midlatitude plasma captured by the high-latitude convection pattern while particle precipitation within the polar cleft may enhance the plasma density further [e.g., *Knudsen*, 1974]. Several mechanisms have been invoked to explain the generation mechanism of plasma patches in the polar cap. For example, high-speed plasma convection and concomitant recombination can segment TOI into smaller patches [e.g., *Taguchi et al.*, 2010]. Temporal changes of reconnection geometry affect the high-latitude convection patterns picking up dayside midlatitude plasma, which leads to polar cap patches [e.g., *Zhang et al.*, 2011]. Electron precipitation in the auroral oval can also generate plasma density irregularities [*Pryse et al.*, 1996]. Similarly, electron precipitation inside the polar cap, which is related with polar cap arcs, can produce localized enhancements of plasma density inside the polar cap [e.g., *Robinson and Mende*, 1990].

[4] Spatial variations of ionospheric plasma density are often accompanied by signatures in the magnetic field strength because of the diamagnetic effect [e.g., *Lühr et al.*, 2003]. Such signatures have been observed in the equatorial and low-latitude ionosphere. Under the assumption of pressure balance across the irregularity the diamagnetic effect, ΔB, can be expressed as:

$$\Delta B = -\frac{k_B \mu_0}{B} \Delta[n_e(T_i + T_e)]. \quad (1)$$

where k_B is the Boltzmann constant, μ_0 the permeability of free space, B is the ambient field strength, n_e is the electron density, T_i and T_e are the ion and electron temperatures, respectively. *Stolle et al.* [2006] successfully reproduced the climatology of EPBs solely based on their magnetic signatures observed by CHAMP. *Park et al.* [2008] found that low-latitude plasma blobs also exhibit similar diamagnetic signatures.

[1]GFZ German Research Center for Geosciences, Potsdam, Germany.
[2]Department of Geoinformatics, Neubrandenburg University, Neubrandenburg, Germany.

Corresponding author: J. Park, GFZ German Research Center for Geoscience, Section 2.3, Telegrafenberg, DE-14473 Potsdam, Germany. (park@gfz-potsdam.de)

0148-0227/12/2012JA018166

[5] Although the diamagnetic signatures of ionospheric plasma irregularities have been thoroughly investigated at low-latitude regions, no such attempt has been made for the high-latitude ionosphere. In this study we will address the diamagnetic signatures of high-latitude plasma irregularities and their relation to field-aligned currents (FACs), as observed by CHAMP. In Section 2 we briefly describe the instruments and the method of automatic event detection. Section 3 presents a climatology of the high-latitude irregularities, as observed by CHAMP. The results are discussed in Section 4, and conclusions are drawn in the final section.

2. Instruments and Event Detection Method

[6] The orbit of CHAMP was near-polar (inclination ~87°) and circular. It started in 2000 at an altitude of about 450 km at launch, and the altitude slowly decayed until the atmospheric reentry in September 2010. The main magnetic payloads of the satellite were the Fluxgate Magnetometer (FGM) and the Overhauser Magnetometer (OVM). The data from these two instruments were cross-calibrated and decimated to produce the high-precision data of geomagnetic field vectors with 1-second sampling. In order to separate ionospheric contributions from the other geomagnetic field terms, we subtracted the Pomme6 magnetic field model (http://www.geomag.us/models/pomme6.html) from the recorded data. The residual vector is projected onto the ambient (model) field direction. The changes of this field component can be deemed as magnetic field strength variations. On this component we further apply a low-pass Savitzky-Golay filter of order 2 and window size of 31 s; corresponding spatial scale of the window size is 7.8 (km/s) × 31 (s) ≈240 (km). Since we are interested in small-scale plasma structures, the low-pass filtered data are subtracted from unfiltered readings, and we obtain a high-pass-filtered time series of the magnetic field strength.

[7] Figure 1 shows the data and processing steps of a sample event on 22 September 2001. The high-pass-filtered magnetic field strength is shown as a solid black line in Figure 1c. We can identify significant fluctuations near 13:42:43 UT. The rectified signal of the fluctuation amplitude is shown in Figure 1d. In this study we only consider filtered/rectified fluctuations above a threshold of 0.25 nT (red dashed line in Figure 1d). The same threshold value was used by *Stolle et al.* [2006] to detect the low-latitude plasma irregularities. Individual events are merged together if their separation is smaller than 60 s. In the presented case the event range is marked by a solid blue line in Figure 1c, where times of positive detection are flagged 1. The ground track of the corresponding CHAMP orbit segment is shown in Figure 1a in geocentric (latitude-longitude) coordinates. The square marks the start time of the segment. In Figure 1b the same track is projected onto the geomagnetic Apex coordinates [*Richmond*, 1995], where the radius corresponds to magnetic latitudes and the azimuth angle to magnetic local time (MLT) in degrees: 0° for midnight, 90° for dawn, and 180° for noon.

[8] As the magnetic field variations may be caused by other processes [e.g., *Heilig et al.*, 2007], we make use of independent means to confirm that a magnetic fluctuation event is actually related to plasma density irregularities. The Digital Ion Drift Meter (DIDM) onboard CHAMP was designed to measure ion density, temperature, and drift velocity, and could have been a stand-alone device to study the high-latitude irregularity climatology. Unfortunately, the instrument was severely degraded during the launch and remained uncalibrated. The electron density readings of DIDM (data rate = 1 Hz) may be scaled locally by comparison with those of the Planar Langmuir Probe (PLP) onboard CHAMP (data rate = 1/15 Hz). However, the scaling factor between the two instruments can drift significantly even within an orbit; e.g., *Park et al.* [2008] scaled the DIDM data piecewise for 10°–20° latitudinal segments. Data gaps and/or spurious data points complicate the situation further. In this study, instead of calibrating the DIDM data for the whole CHAMP lifetime, we make use of the raw plasma density readings of DIDM at 1-second sampling. The DIDM readings are only used for calculating the correlation coefficients with the magnetic field data, which are unaffected by missing scaling factors. The effect of slowly drifting scaling factors is expected to be small because the mean scale size of the events detected by the above mentioned method is quite small (<5° in geographic latitude (GLAT) ~<80 second duration).

[9] In Figure 1e the DIDM data (solid black line) are scaled locally by the PLP readings (red dots) for demonstration purpose. The same high-pass filter as applied to the FGM data (Figure 1c) is used for the DIDM plasma data (Figure 1f), and then the result is correlated with the magnetic data for the time of the detected event (marked by a solid red bar in Figure 1d). If the correlation coefficient (shown as 'R' in Figure 1c) is significantly negative, we can consider the magnetic fluctuations to be of diamagnetic origin [e.g., *Park et al.*, 2008]. In our study the threshold for R is -0.6; otherwise we discard the magnetic fluctuation event. If an event contains a data gap larger than 1 second, we also drop the event. Similarly, events whose magnetic latitude (MLAT) is lower than 30° are not considered.

[10] For comparison, Figure 1g shows collocated FACs deduced from CHAMP magnetic field readings (positive upward) [*Ritter and Lühr*, 2006]. Small-scale FACs with wavelength of several tens of kilometers are plotted in black. Large-scale FACs (>200 km) are plotted as dashed red line. Concurrent with the large electron density irregularity (near 13:42:43 UT) a burst of intense small-scale FACs occurs. Also later density variations with smaller amplitudes (near 13:43:43 UT) are accompanied by small-scale FACs. The intense FAC burst near 13:42:43 UT is mostly imbedded in a transition region from downward to upward large-scale FAC sheet (dashed red curve).

3. Statistical Results

[11] For determining the characteristics and climatology of the high-latitude plasma irregularity we applied the detection algorithm described above to the CHAMP data for the years 2001–2010, which comprise in total more than 40000 orbits. Numbers of positively detected events are listed in Table 1. Event numbers are from the two periods: 2001–2005 and 2006–2010 representing solar maximum and solar minimum conditions, respectively. Some features of the event occurrences are immediately evident. First, the total number of events in 2001–2005 is much larger than in 2006–2010.

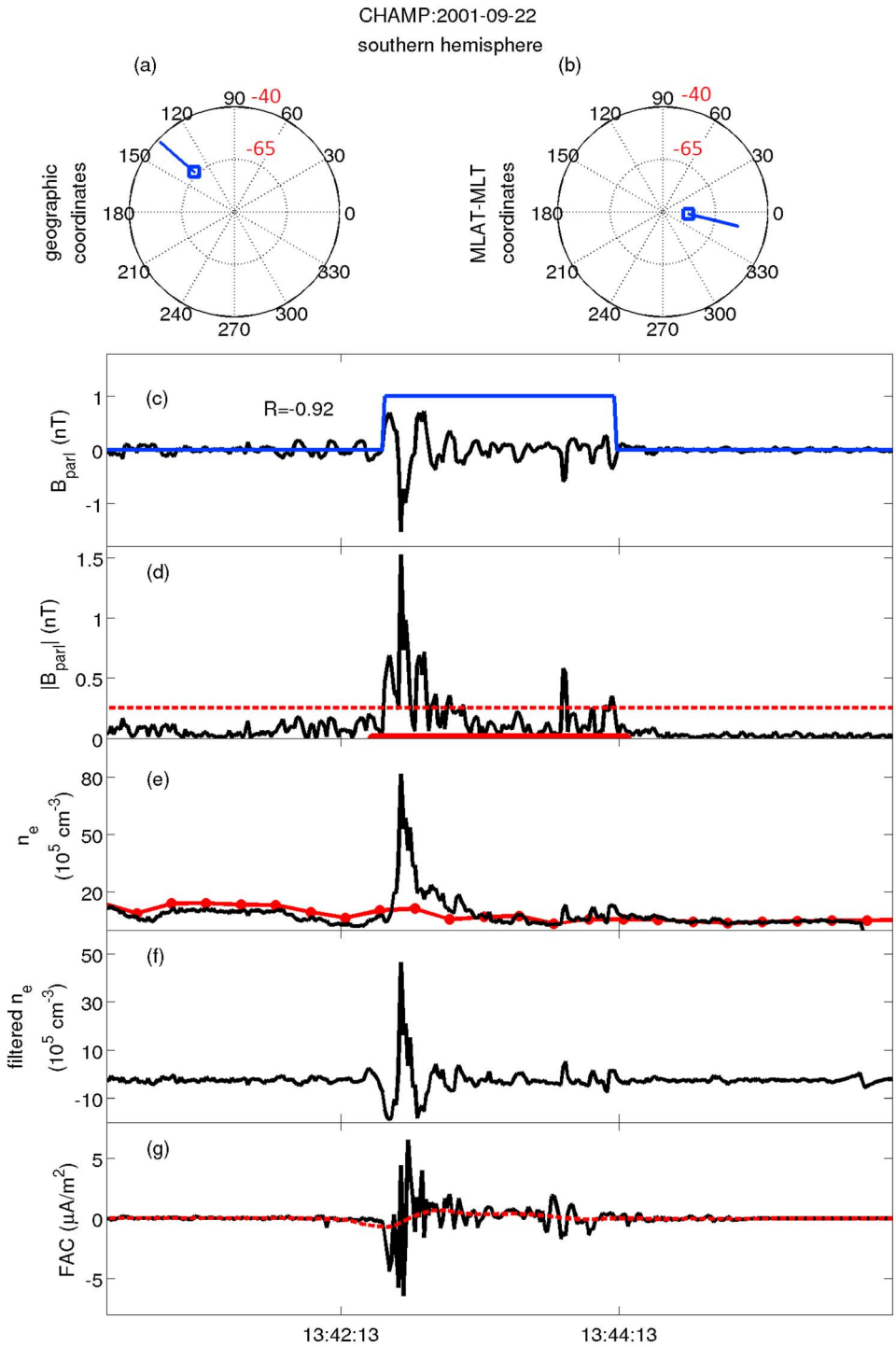

Figure 1. An example of the diamagnetic fluctuation of geomagnetic field strength: (a) ground track of CHAMP in geocentric coordinates, (b) ground track of CHAMP in geomagnetic coordinates, (c) filtered magnetic field strength, (d) filtered/rectified magnetic field strength, and (e) plasma density as observed by DIDM (black), which is rescaled by the calibrated PLP data (red), (f) filtered plasma density, and (g) small-scale (black) and large-scale (red) FAC density.

Second, the total number of events in June solstice is much smaller than in the other seasons. This trend is less pronounced during solar minimum years. The overall event numbers are comparable in both hemispheres.

[12] For further analysis we sort the data points into bins of MLAT versus MLT, separately for season, hemisphere, *AE* index, and year. In each bin the occurrence rate is calculated as the ratio between the number of FGM data points

Table 1. Numbers of Positively Detected Events[a]

	Northern Hemisphere		Southern Hemisphere	
	2001–2005	2006–2010	2001–2005	2006–2010
Equinox	1136	209	1177	196
June solstice	492	244	586	128
December solstice	1666	217	1069	335

[a]Event numbers are from the two periods: 2001–2005 and 2006–2010 representing solar maximum and solar minimum conditions, respectively.

within plasma irregularity events to the total number of FGM data points. Note that FGM data points without corresponding DIDM data are excluded from both the numerator and the denominator of the ratio; i.e. those data points are not considered in the statistics. For the binning we use equal-area cells (222 × 232 km) as described by *Lühr et al.* [2007].

[13] Figure 2 shows the average occurrence distribution of irregularities over all the years considered. The probability for an event is much higher during magnetically active times with the auroral index $AE \geq 200$ nT (Figure 2, bottom) than during quiet periods (Figure 2, top). Irregularities are found predominantly at MLAT typical for the auroral oval. Particularly outstanding in both hemispheres is the high rate in the cusp region: reaching 1.2 % for quiet periods (Figure 2, top) and reaching 2.6 % for disturbed periods (Figure 2, bottom). A secondary maximum in the pre-midnight sector of the northern hemisphere may be related to substorm activity: reaching 0.8 % for the quiet period (Figure 2, top) and reaching 1.8 % for the disturbed period (Figure 2, bottom). Those features are less conspicuous in the southern hemisphere: reaching 0.4 % for the quiet period (Figure 2, top) and reaching 0.8 % for the disturbed period (Figure 2, bottom). Overall, the occurrence rate amounts to a few percent. This magnitude is comparable to the EPB occurrence rate shown in *Stolle et al.* [2006, Figure 7] and *Xiong et al.* [2010,

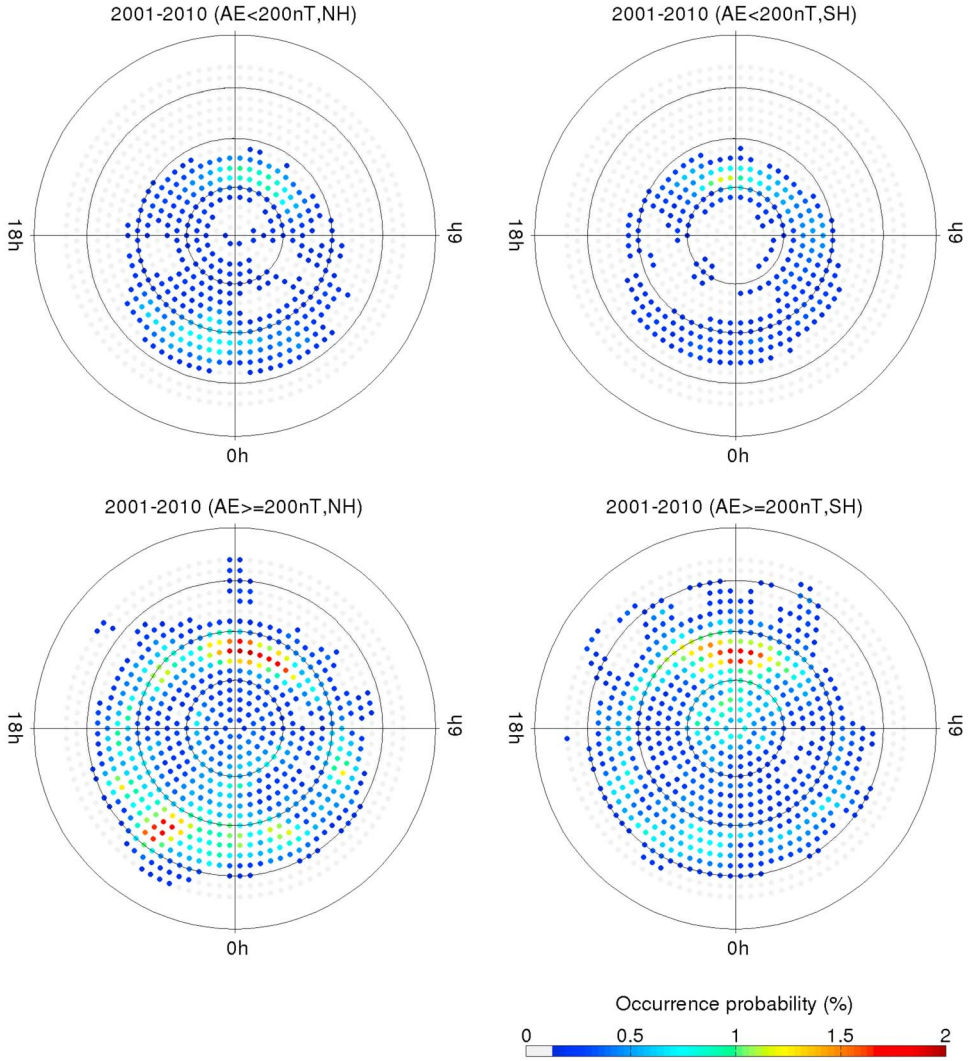

Figure 2. Climatology of the plasma density irregularities in 2001–2010. The distributions in magnetic coordinates for geomagnetically (top) quiet and (bottom) active periods in the (left) northern and (right) southern hemispheres. Concentric circles mark latitudes at 10° spacing.

Figure 9], implying that the high-latitude plasma irregularities occur nearly as frequently as EPBs.

[14] Next, we are interested in the seasonal dependence of the irregularity occurrence. From Table 1 we know that more events occurred during the early years of the CHAMP mission before 2005 than after 2006. From Figure 2 we learned about the positive dependence of the events on geomagnetic activity. The occurrence probabilities in Figure 3 are thus separated by seasons for favorable conditions (i.e., for geomagnetically active periods in 2001–2005). During equinoctial months the occurrence distribution is quite similar in the two hemispheres at MLAT typical for the auroral oval. Outstanding rates show up at the cusp: reaching 4.0 % (3.5 %) in the northern (southern) hemisphere. For months around June solstice event rates are largely reduced in both hemispheres. Quite outstanding is again the cusp region in the southern hemisphere (local winter) : reaching 3.2 %. Large hemispheric differences are observed during December solstice months. While in the northern hemisphere (local winter) we find a peak event rate around the cusp (reaching 5.0 %) and in the pre-midnight sector (reaching 4.0 %), the overall occurrence rate in the south (local summer) is low with a global maximum around the cusp (reaching 1.9 %).

[15] Since plasma irregularities can disturb GPS navigation signals, it may be of interest to know the geographic distribution of the occurrence rate. Figure 4 shows the event rates for geomagnetically active periods in 2001–2005. The blue dotted lines denote MLAT. In the northern hemisphere (Figure 4, left) we find that the occurrence rate is high (reaching about 1.0 %) between 65° and 75° MLAT. It is interesting that the events are concentrated in the American and European continents while the rates over the East Siberian landmass are rather low. In the southern hemisphere regions of high occurrence rate (reaching about 1.0 %) are not strictly confined to latitudes between 65° and 75° MLAT. Nevertheless, the distribution is significantly biased toward the 120° geographic longitude (GLON) sector, which is close to GLON of the geomagnetic pole. The occurrence rate below 60° MLAT is quite low (represented in gray). Therefore, we can conclude that the distribution of plasma irregularity occurrence is aligned better with MLAT (blue dashed lines) than with GLAT (thin black grids). This is true for both hemispheres.

4. Discussion

[16] Here we have presented a comprehensive survey of local plasma irregularities based on their diamagnetic signature. According to visual inspection of arbitrarily selected sample events, these irregularities with scale sizes below some hundred kilometers are commonly characterized by electron density enhancements. In response we find depletions in magnetic field strength of about 1 nT (see Figure 1). In a global survey of compressional signal power in the frequency range 20–70 mHz (15–50s period), based on CHAMP data, *Heilig et al.* [2007] found three activity regions [see *Heilig et al.*, 2007, Figure 8]. The one around noon at low and midlatitude was related to compressional upstream waves, which was the main topic of that paper. Another active region was located at low latitudes during post-sunset hours. This was attributed by *Heilig et al.* [2007] to EPBs [*Stolle et al.*, 2006]. The third activity region was confined to the auroral latitudes. We believe that this third region is caused to a large extent by the plasma irregularities we study here. The high-latitude (>60° MLAT) part of *Heilig et al.* [2007, Figure 8] (i.e. the third activity region) is in reasonable agreement with our Figure 2 (bottom), as addressed in the three aspects below. First, in both hemispheres we find peak activities in the cusp region. Second, in the northern hemisphere there appears a clear secondary peak in the pre-midnight sector, which is nearly comparable in strength to the cusp peak. Third, in the southern hemisphere this secondary peak is significantly weaker than the cusp peak. This secondary peak in the southern hemisphere is clearly seen in *Heilig et al.* [2007, Figure 8], and can also be identified in our Figure 2 though not as conspicuous. Based on the agreement between the two independent studies we suggest that a significant part of the total field variations in the CHAMP magnetic field data at high latitude is caused by spatial structures of plasma. In this study we required independent confirmation by plasma measurements, thereby had to ignore magnetic fluctuation events without corresponding DIDM data. The number of those neglected events is comparable to the total number listed in Table 1.

[17] A number of studies have investigated high-latitude ionospheric irregularities using ground-based observations. Due to the sparseness of observatories those observations reflect not only the temporal variation of irregularity occurrences, but are also affected by the diurnal entrance and exit of the observing site into a region of enhanced occurrence rates (for example, the auroral oval) (see *Aarons* [1997, Figure 2b] and related discussions). Our results, which are based on CHAMP satellite observations, provide nearly continuous spatial coverage. Hence, we expect that our results are closer to the true spatial/temporal climatology of ionospheric irregularities at high latitudes.

[18] Important climatological features of the irregularity occurrence can be deduced from Figures 2 and 3. Periods of high solar activity (2001–2005) and high auroral activity ($AE > 200$ nT) are generally preferred for the event occurrence. At least the first condition indicates that the background state of the upper atmosphere plays a role for the generation of the irregularity. Quite interesting are the seasonal variations in the two hemispheres, as shown in Figure 3, and the globally low event rate around June solstice. It is known that both the ionosphere and the thermosphere experience an annual variation with minima around July [e.g., *Rishbeth et al.*, 2000; *Müller et al.*, 2009] and maxima during equinoxes. By considering these conditions we speculate that a denser upper atmosphere supports the creation of plasma irregularities. This is also consistent with the enhanced event rate during higher solar fluxes, as mentioned above.

[19] There seems to be an additional effect caused by sunlight. Irregularities are caused more easily under local darkness (see the local winter preference in Figure 3). This can explain the large difference between occurrence probabilities in the two hemispheres around December solstice. In the northern hemisphere favorable local darkness conditions (around December solstice) are paired with an enhanced background density, while in the southern hemisphere the

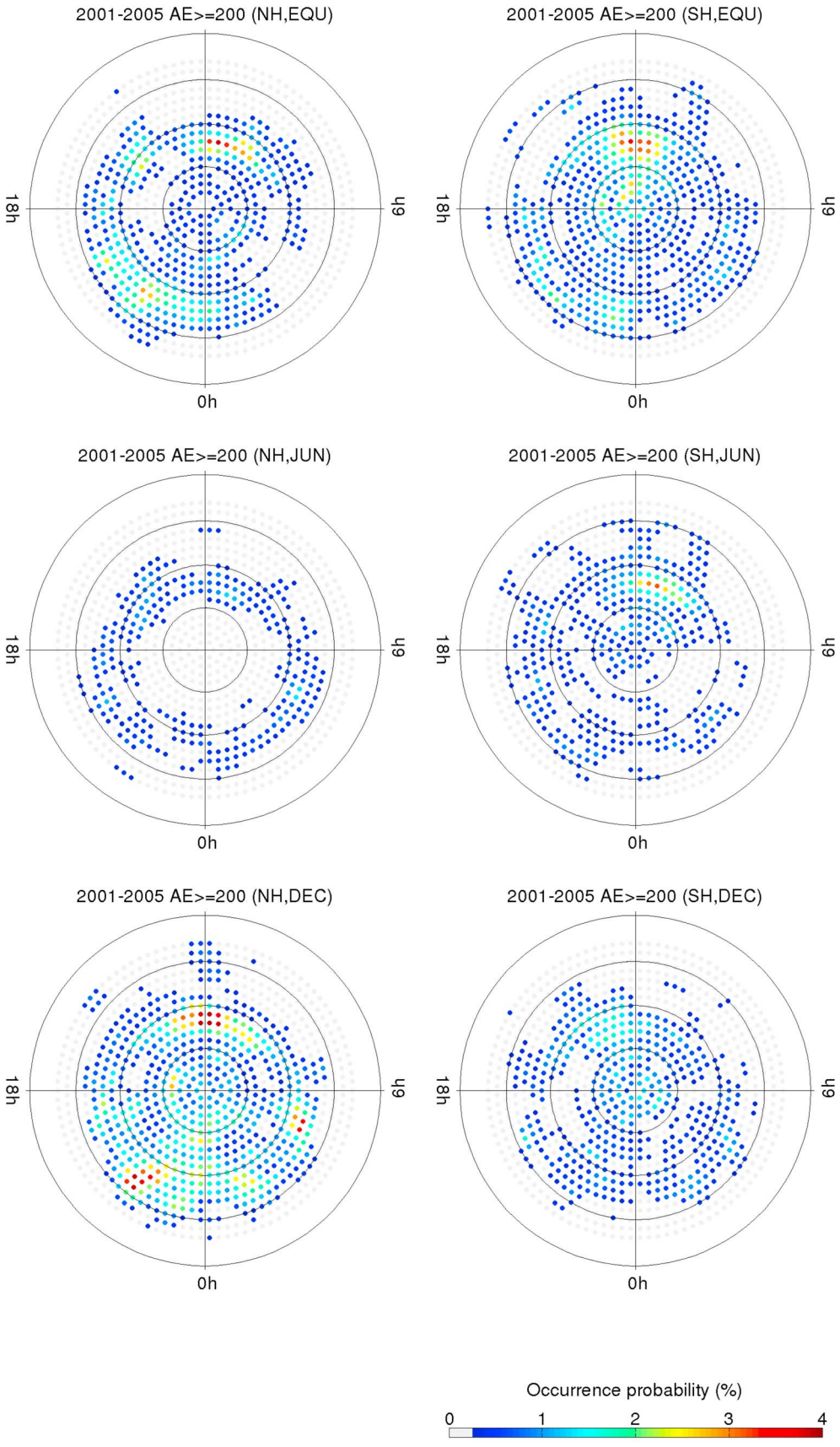

Figure 3. Climatology of the plasma density irregularities during geomagnetically active periods in 2001–2005. (top) Equinox, (middle) June solstice, and (bottom) December solstice.

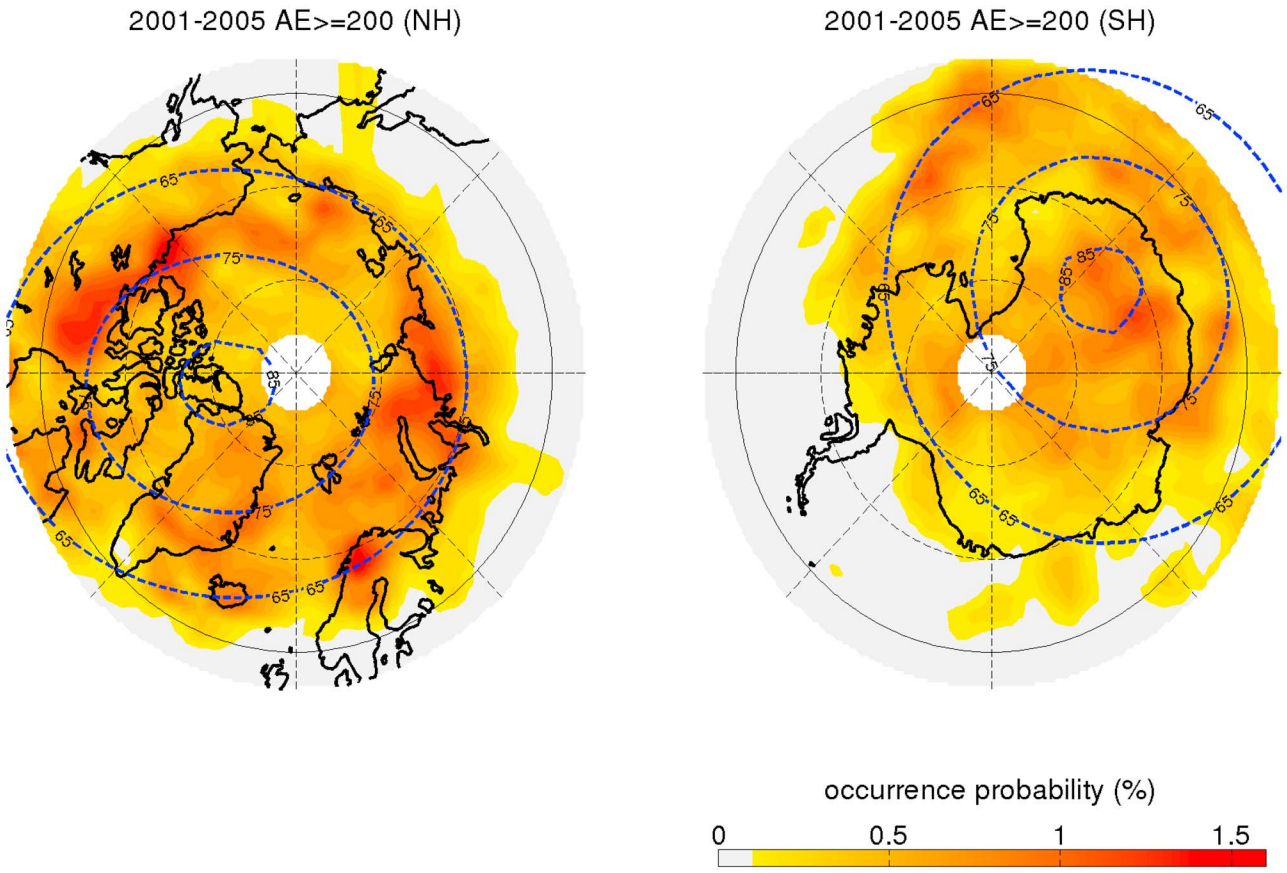

Figure 4. Distribution of plasma density irregularities during geomagnetically active periods in 2001–2005 shown in geocentric coordinates for the (left) northern and (right) southern hemispheres. The blue dotted lines denote the Apex latitude [*Richmond*, 1995].

two conditions compensate each other. Similarly, we can explain the low occurrence probabilities in the northern hemisphere during June solstice months by the combined effect of low background density and continuous sunlight. In the southern hemisphere these effects compensate each other again. As a consequence we find a much weaker seasonal variation in the southern hemisphere than in the northern hemisphere.

[20] Our observations are in general agreement with the GPS phase scintillation climatology as reported by *Prikryl et al.* [2011] for solar minimum years (2008–2009). They found that the scintillation occurs predominantly in the cusp and in the nightside auroral latitudes [*Prikryl et al.*, 2011, Figure 6]. With increasing geomagnetic activity the occurrence rate becomes stronger and the scintillation latitude moves equatorward [*Prikryl et al.*, 2011, Figure 8]. The scintillation around the dayside cusp shows an annual variation with the maximum in the northern autumn-winter [*Prikryl et al.*, 2011, Figure 6]. As their results were obtained in the northern hemisphere, the autumn-winter maximum is compatible with the seasonal (local winter preference) and annual (December solstice preference) variation in our results. The only difference from our results is that their scintillation probability at the nightside auroral latitudes exhibited a semi-annual variation with the maximum occurrence at equinoxes. Note that our observations and those of *Prikryl et al.* [2011] correspond to different altitude ranges. The GPS scintillation can be affected by both the E- and F-layer irregularities, especially during enhanced geomagnetic activity [e.g., *Aarons et al.*, 1995; *Aarons*, 1997], whereas the CHAMP/FGM detects plasma pressure irregularities at the orbit altitude (generally above the F-region peak). *Prikryl et al.* [2011] suggested that scintillations at nightside auroral latitudes originate from particle precipitations. It is well known that softer electron precipitation causes ionization at higher altitudes. If softer and harder components of auroral precipitations exhibit different seasonal/LT dependencies, this might be the explanation for the slight difference between *Prikryl et al.* [2011] and our results at nightside auroral latitudes.

[21] It is worth discussing further why the pre-midnight peak of occurrence rate is conspicuous/inconspicuous in the northern/southern hemisphere, respectively (see Figure 2). Using equinoctial airglow images taken at conjugate areas in the Alaskan meridian *Stenbaek-Nielsen et al.* [1973] demonstrated that the auroral activity is generally more frequent and more intense in the northern hemisphere than in the southern. The hemispheric asymmetry of the pre-midnight

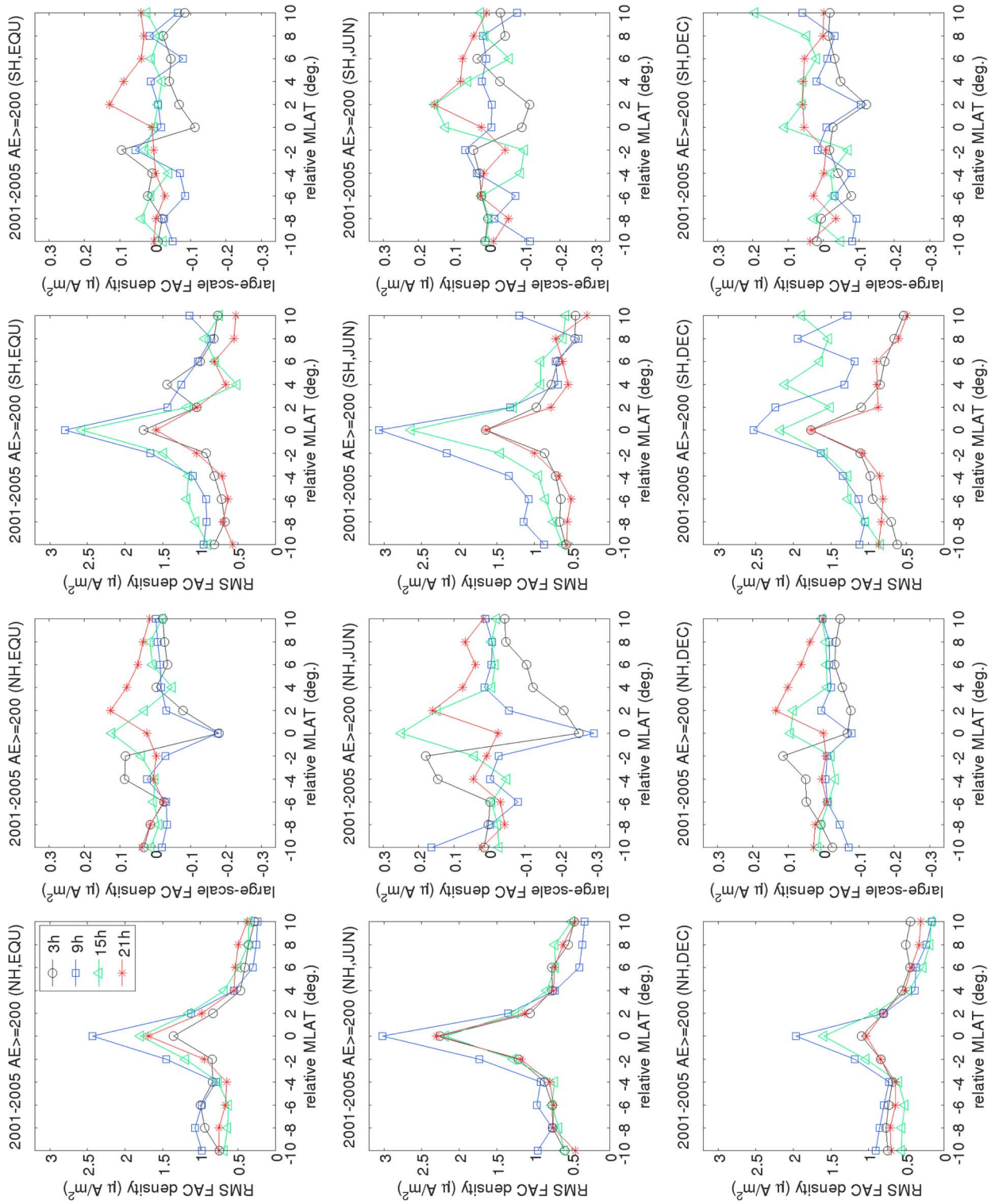
2001-2005 AE>=200 (NH,EQU)
2001-2005 AE>=200 (NH,JUN)
2001-2005 AE>=200 (NH,DEC)
2001-2005 AE>=200 (SH,EQU)
2001-2005 AE>=200 (SH,JUN)
2001-2005 AE>=200 (SH,DEC)
RMS FAC density (μ A/m²)
large-scale FAC density (μ A/m²)
relative MLAT (deg.)
3h
9h
15h
21h

Figure 5

occurrence peak in our Figure 2 may be related to the difference in particle precipitation being also responsible for the airglow asymmetry. On the contrary, *Luan et al.* [2010] reported that no hemispheric difference can be found in auroral hemispheric power under local winter conditions, which seems to be at odds with our results and *Stenbaek-Nielsen et al.* [1973]. More theoretical and observational studies are needed to clarify the hemispheric asymmetry in plasma irregularity occurrence rates at pre-midnight auroral latitudes.

[22] In a quest for the processes responsible for the generation of the ionospheric irregularities at CHAMP altitude we had a closer look at collocated FACs. Already from Figure 1 it is evident that the plasma irregularity is accompanied by a burst of small-scale FACs. In order to derive statistically relevant results we have performed superposed epoch analyses (SEA). For these analyses the center MLAT of each event is taken as the key MLAT and concurrent FAC estimates are stacked according to that reference. Figure 5 shows the results of SEA applied to small-scale and large-scale FACs separately. In case of small scales (odd columns in Figure 5) the root-mean square (RMS) value of the amplitude computed over orbital arcs of about 150 km is used for SEA. In case of large scales (even columns in Figure 5) the current density readings are used directly, where positive (negative) values indicate upward (downward) currents. Events from the two hemispheres are treated separately (columns 1–2 and 3–4). In addition, the data have been divided into the three seasons (shown in different rows) and 6-hour MLT sectors (shown with different line colors).

[23] A prominent result of the SEA is that plasma irregularities are commonly accompanied by bursts of small-scale FACs. This is true for all seasons and all MLTs. As expected, small-scale FACs are strongest in the prenoon sector (09 h MLT), followed by the afternoon sector (15 h MLT). Interestingly, June solstice is the preferred seasons for these FAC, independent of hemisphere. At a given MLT range, however, the small-scale FACs at the key MLAT seem to have generally comparable amplitude in both hemispheres for all the seasons. On the nightside these FACs have amplitudes about half as large as on the dayside.

[24] Rather different signatures emerge from the large-scale FACs. The key MLAT for dawnside sectors (03 and 09 MLT) generally coincides with the peak in downward FACs. Conversely, the key MLAT for the afternoon MLT sector (15 MLT) is by and large located at the peak of upward FACs. In the pre-midnight sector (21 MLT) the upward FAC peak appears about 2° poleward of the key MLAT. This FAC signature clearly indicates that our plasma irregularities prefer to form in connection with the Region 1 (R1) FAC regime. About 2°–4° equatorward of the key latitude large-scale FACs with opposite polarity appear: upward and downward at the dawnside (03 and 09 MLT) and in the afternoon (15 MLT) sector, respectively. These oppositely directed FACs are consistent with the R2 regime. In a dedicated study *Rother et al.* [2007] had investigated the features of very small (km-scale) FACs. They also performed a SEA between small- and large-scale FACs. *Rother et al.* [2007, Figure 15] reveal average signatures of large-scale FACs for the different MLT sectors, which are consistent with our Figure 5. They also conclude a relation of small-scale FAC with the R1 FAC. In general R1 FAC are mapped to the low-latitude boundary layer and boundary plasma sheet while R2 FAC includes central plasma sheet and ring current region [e.g., *Wing et al.*, 2010]. As precipitation from the central plasma sheet is generally more energetic (several keV) and unstructured [e.g., *de la Beaujardiere et al.*, 1993], it can hardly generate F-region plasma irregularities. On the other hand, the electrons in the boundary plasma sheet and cusp/mantle have softer spectra, they are more efficient in changing the F-region plasma density. Therefore, precipitation related to R1 FACs is more likely to generate F-region irregularities than that of the R2 FAC regime.

[25] From Figure 5 we can conclude that small-scale FACs play a major role in forming the irregularity, but there seem to be other modulating factors that cause the difference in seasonal patterns between FAC amplitudes and irregularity occurrence probabilities. Moreover, a non-negligible number of irregularities are found in the polar cap region; see Figure 3 (top right). These events are not expected to be accompanied by small-scale FACs. They are likely to be transported into that region by high-latitude plasma convection [e.g., *Crowley et al.*, 2000].

5. Summary

[26] Using the geomagnetic field and relative plasma density variations observed by CHAMP during the years 2001–2010 we have investigated the climatology of ionospheric irregularities in the high-latitude ionospheric F-region. From the observations we can draw the following conclusions:

[27] 1. The spatial distribution of the occurrence rate generally peaks along auroral latitudes around the pole, but it is not uniform zonally. The occurrence rate of the ionospheric irregularities exhibits a maximum at the dayside cusp and pre-midnight ionosphere.

[28] 2. The occurrence rate increases with solar activity. The probability is higher during auroral active periods ($AE \geq 200$) than for quiet periods ($AE < 200$). The region of high occurrence rate expands equatorward with increasing *AE*.

[29] 3. During active periods ($AE \geq 200$ in 2001–2005) there are higher occurrence probabilities in local winter than in local summer (i.e. seasonal variation). The overall occurrence rate is smallest around June solstice and largest around December solstice (i.e. annual variation).

[30] 4. The ionospheric irregularities are commonly accompanied by bursts of small-scale FACs.

[31] 5. The ionospheric irregularities occur preferably in the R1 FAC regime.

Figure 5. Superposed epoch analyses of FACs around the occurrence of plasma density irregularities. From top to bottom the rows correspond to equinox, June solstice, and December solstice. The first and second columns stand for the northern hemisphere, and the third and fourth columns stand for the southern hemisphere. Odd-numbered columns present root-mean square values of small-scale FAC. Even-numbered columns show large-scale FACs. Different colors are used for different MLT sectors.

[32] **Acknowledgments.** The authors thank M. Noja for valuable discussions. The CHAMP mission was sponsored by the Space Agency of the German Aerospace Center (DLR) through funds of the Federal Ministry of Economics and Technology, following a decision of the German Federal Parliament (grant code 50EE0944). The data retrieval and operation of the CHAMP satellite by the German Space Operations Center (GSOC) is acknowledged.

[33] Robert Lysak thanks the reviewers for their assistance in evaluating this paper.

References

Aarons, J. (1997), Global positioning system phase fluctuations at auroral latitudes, *J. Geophys. Res.*, *102*(A8), 17,219–17,231.

Aarons, J., H. E. Whitney, E. MacKenzie, and S. Basu (1981), Microwave equatorial scintillation intensity during solar maximum, *Radio Sci.*, *16*(5), 939–945, doi:10.1029/RS016i005p00939.

Aarons, J., L. Kersley, and A. S. Rodger (1995), The sunspot cycle and 'auroral' F layer irregularities, *Radio Sci.*, *30*(3), 631–638.

Bhattacharyya, A., T. L. Beach, S. Basu, and P. M. Kintner (2000), Nighttime equatorial ionosphere: GPS scintillations and differential carrier phase fluctuations, *Radio Sci.*, *35*(1), 209–224, doi:10.1029/1999RS002213.

Crowley, G., A. J. Ridley, D. Deist, S. Wing, D. J. Knipp, B. A. Emery, J. Foster, R. Heelis, M. Hairston, and B. W. Reinisch (2000), Transformation of high-latitude ionospheric F region patches into blobs during the March 21, 1990, storm, *J. Geophys. Res.*, *105*(A3), 5215–5230, doi:10.1029/1999JA900357.

de la Beaujardiere, O., J. Watermann, P. Newell, and F. Rich (1993), Relationship between Birkeland current regions, particle precipitation, and electric fields, *J. Geophys. Res.*, *98*(A5), 7711–7720, doi:10.1029/92JA02005.

Heilig, B., H. Lühr, and M. Rother (2007), Comprehensive study of ULF upstream waves observed in the topside ionosphere by CHAMP and on the ground, *Ann. Geophys.*, *25*, 737–754, doi:10.5194/angeo-25-737-2007.

Kil, H., and R. A. Heelis (1998), Global distribution of density irregularities in the equatorial ionosphere, *J. Geophys. Res.*, *103*(A1), 407–417, doi:10.1029/97JA02698.

Knudsen, W. C. (1974), Magnetospheric convection and the high-latitude F 2 ionosphere, *J. Geophys. Res.*, *79*(7), 1046–1055, doi:10.1029/JA079i007p01046.

Luan, X., W. Wang, A. Burns, S. Solomon, Y. Zhang, and L. J. Paxton (2010), Seasonal and hemispheric variations of the total auroral precipitation energy flux from TIMED/GUVI, *J. Geophys. Res.*, *115*, A11304, doi:10.1029/2009JA015063.

Lühr, H., M. Rother, S. Maus, W. Mai, and D. Cooke (2003), The diamagnetic effect of the equatorial Appleton anomaly: Its characteristics and impact on geomagnetic field modeling, *Geophys. Res. Lett.*, *30*(17), 1906, doi:10.1029/2003GL017407.

Lühr, H., S. Rentz, P. Ritter, H. Liu, and K. Häusler (2007), Average thermospheric wind patterns over the polar regions, as observed by CHAMP, *Ann. Geophys.*, *25*, 1093–1101.

Müller, S., H. Lühr, and S. Rentz (2009), Solar and magnetospheric forcing of the low latitude thermospheric mass density as observed by CHAMP, *Ann. Geophys.*, *27*, 2087–2099, doi:10.5194/angeo-27-2087-2009.

Nishioka, M., S. Basu, S. Basu, C. E. Valladares, R. E. Sheehan, P. A. Roddy, and K. M. Groves (2011), C/NOFS satellite observations of equatorial ionospheric plasma structures supported by multiple ground-based diagnostics in October 2008, *J. Geophys. Res.*, *116*, A10323, doi:10.1029/2011JA016446.

Park, J., C. Stolle, H. Lühr, M. Rother, S.-Y. Su, K. W. Min, and J.-J. Lee (2008), Magnetic signatures and conjugate features of low-latitude plasma blobs as observed by the CHAMP satellite, *J. Geophys. Res.*, *113*, A09313, doi:10.1029/2008JA013211.

Prikryl, P., P. T. Jayachandran, S. C. Mushini, and R. Chadwick (2011), Climatology of GPS phase scintillation and HF radar backscatter for the high-latitude ionosphere under solar minimum conditions, *Ann. Geophys.*, *29*, 377–392, doi:10.5194/angeo-29-377-2011.

Pryse, S. E., L. Kersley, and I. K. Walker (1996), Blobs and irregularities in the auroral ionosphere, *J. Atmos. Terr. Phys*, *58*(1), 205–215, doi:10.1016/0021-9169(95)00030-5.

Richmond, A. D. (1995), Ionospheric electrodynamics using magnetic apex coordinates, *J. Geomagn. Geoelectr.*, *47*, 191–212.

Rishbeth, H., I. C. F. Müller-Wodarg, L. Zou, T. J. Fuller-Rowell, G. H. Millward, R. J. Moffett, D. W. Idenden, and A. D. Aylward (2000), Annual and semiannual variations in the ionospheric F2-layer: II. Physical discussion, *Ann. Geophys.*, *18*, 945–956, doi:10.1007/s00585-000-0945-6.

Ritter, P., and H. Lühr (2006), Search for magnetically quiet CHAMP polar passes and the characteristics of ionospheric currents during the dark season, *Ann. Geophys.*, *24*, 2997–3009, doi:10.5194/angeo-24-2997-2006.

Robinson, R. M., and S. B. Mende (1990), Ionization and electric field properties of auroral arcs during magnetic quiescence, *J. Geophys. Res.*, *95*(A12), 21,111–21,121, doi:10.1029/JA095iA12p21111.

Rother, M., K. Schlegel, and H. Lühr(2007), CHAMP observation of intense kilometer-scale field-aligned currents, evidence for an ionospheric Alfvén resonator, *Ann. Geophys.*, *25*, 1603–1615, doi:10.5194/angeo-25-1603-2007.

Seo, J., T. Walter, and P. Enge (2011), Availability impact on GPS aviation due to strong ionospheric scintillation, *IEEE Trans. Aerosp. Electron. Syst.*, *47*(3), 1963–1973.

Stenbaek-Nielsen, H. C., E. M. Wescott, T. N. Davis, and R. W. Peterson (1973), Differences in auroral intensity at conjugate points, *J. Geophys. Res.*, *78*(4), 659–671, doi:10.1029/JA078i004p00659.

Stolle, C., H. Lühr, M. Rother, and G. Balasis (2006), Magnetic signatures of equatorial spread F as observed by the CHAMP satellite, *J. Geophys. Res.*, *111*, A02304, doi:10.1029/2005JA011184.

Su, S.-Y., C. H. Liu, H. H. Ho, and C. K. Chao (2006), Distribution characteristics of topside ionospheric density irregularities: Equatorial versus midlatitude regions, *J. Geophys. Res.*, *111*, A06305, doi:10.1029/2005JA011330.

Taguchi, S., K. Hosokawa, S. Suzuki, A. S. Yukimatu, and N. Sato (2010), Initial development of HF radar polar patch caused by azimuthal flow burst in the cusp, *J. Geophys. Res.*, *115*, A05305, doi:10.1029/2009JA014631.

Wing, S., S. Ohtani, P. T. Newell, T. Higuchi, G. Ueno, and J. M. Weygand (2010), Dayside field-aligned current source regions, *J. Geophys. Res.*, *115*, A12215, doi:10.1029/2010JA015837.

Xiong, C., J. Park, H. Lühr, C. Stolle, and S. Y. Ma (2010), Comparing plasma bubble occurrence probabilities at CHAMP and GRACE altitudes during high and low solar activity, *Ann. Geophys.*, *28*, 1647–1658, doi:10.5194/angeo-28-1647-2010.

Xiong, C., H. Lühr, S. Y. Ma, C. Stolle, and B. G. Fejer (2012), Features of highly structured equatorial plasma irregularities deduced from CHAMP observations, *Ann. Geophys.*, *30*, 1259–1269, doi:10.5194/angeo-30-1259-2012.

Zhang, Q.-H., et al. (2011), On the importance of interplanetary magnetic field $|B_y|$ on polar cap patch formation, *J. Geophys. Res.*, *116*, A05308, doi:10.1029/2010JA016287.